Crystal structure and spectroscopic characterization of (E)-2-(((4-bromo-2-(trifluoromethoxy)phenyl)imino)methyl)-4-nitrophenol: A combined experimental and computational study

ARTICLE *in* JOURNAL OF MOLECULAR STRUCTURE · APRIL 2014

Impact Factor: 1.6 · DOI: 10.1016/j.molstruc.2014.01.079

Journal of Molecular Structure 1063 (2014) 295–306

Contents lists available at ScienceDirect

Journal of Molecular Structure

journal homepage: www.elsevier.com/locate/molstruc

Crystal structure and spectroscopic characterization of (E)-2-(((4-bromo-2-(trifluoromethoxy)phenyl)imino)methyl)-4-nitrophenol: A combined experimental and computational study

Ömer Tamer [a], Necmi Dege [b], Güneş Demirtaş [b], Davut Avcı [a,*], Yusuf Atalay [a], Mustafa Macit [c], Songül Şahin [c]

[a] Sakarya University, Faculty of Arts and Sciences, Department of Physics, 54187 Sakarya, Turkey
[b] Ondokuz Mayıs University, Faculty of Arts and Sciences, Department of Physics, 55139 Samsun, Turkey
[c] Ondokuz Mayıs University, Faculty of Arts and Sciences, Department of Chemistry, 55139 Samsun, Turkey

HIGHLIGHTS

- A novel compound was synthesized and characterized experimentally.
- DFT calculations were carried out.
- The formation of weak H-bonding was proved by NBO analysis.
- The title compound can be used as an effective NLO material.

ARTICLE INFO

Article history:
Received 22 October 2013
Received in revised form 18 January 2014
Accepted 20 January 2014
Available online 3 February 2014

Keywords:
(E)-2-(((4-bromo-2-(trifluoromethoxy)phenyl)imino)methyl)-4-nitrophenol
Crystal structure
Vibrational spectroscopy
DFT calculations
NLO and NBO analysis

ABSTRACT

A novel compound crystallizes in the triclinic space group *P*−*1* with $a = 7.674(4)$ Å, $b = 12.584(6)$ Å, $c = 15.921(6)$ Å, $\alpha = 89.62(4)°$, $\beta = 84.34(4)°$, $\gamma = 73.77(4)°$ and $Z = 4$. This compound contains Schiff base and rings of molecule has (E) configuration with respect to the central C=N double bond. The crystal structure has the intramolecular O—H···N and the intermolecular C—H···O hydrogen bonds. Molecular modeling of the title compound was done by using density functional theories (DFT). Detailed vibrational assignments have been made on the basis of potential energy distribution (PED). Additionally, chemical shift assignments, investigations of thermodynamical parameters and plotting of molecular electrostatic potential surfaces have been performed with the help of DFT method. In order to understand the electronic transitions of the title compound, time dependent DFT (TD-DFT) calculations were performed in gas phase. The dipole moment, linear polarizabilities, anisotropy and first hyperpolarizabilities values have been also computed using the same method.

1. Introduction

Compounds which contain XC=NY structure (X and Y are the organic side chains) are known as Schiff bases, which are generally synthesized from the condensation of primary amines and active carbonyl groups. Schiff base compounds exhibit interesting photochromic and thermochromic features in the solid state. Photo- and thermochromism arise by means of proton transfer from the hydroxyl O atom to the imine N atom [1,2]. Such proton-exchanging materials can be used for the design of various molecular electronic devices [3,4]. In general, schiff bases display two possible tautomeric forms, the enol-imine compounds which contain a hydroxyl group bounding to a carbon atom in the benzene ring (OH) and the keto-amine (NH) forms (see Fig. 1).

Because of similarity to biological species and relatively small size, phenol derivates are very interesting molecules for theoretical studies. It is well known that phenols are organic compounds which contain a hydroxyl group bounding to a carbon atom in the benzene ring. Additionally, nitroaromatic compounds are effectively used in the different field such as pharmaceuticals, pesticides, plasticizers, azo dyes and explosives industries [5,6]. It is reported that nitrophenolic compounds can accumulate in the soil as a result of hydrolysis of several insectides such as parathion, methyl parathion and fenitrothion. Nitrophenolic compounds are used as anti-bacterial and anti-septic and also for the treatment of surgical instrument and bandaging materials [7].

* Corresponding author. Tel.: +90 264 295 6097; fax: +90 264 295 5950.
E-mail address: davci@sakarya.edu.tr (D. Avcı).

http://dx.doi.org/10.1016/j.molstruc.2014.01.079
0022-2860/

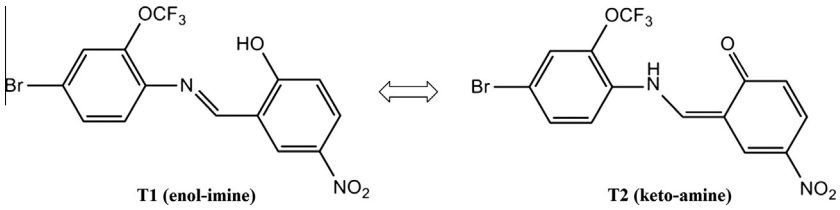

Fig. 1. Tautomeric forms (enol-imine and keto-amine) of the title compound.

Various spectroscopic studies for the phenol derivates have been reported in the literature [8–10]. However, to the best of our knowledge, neither quantum chemical calculations nor the experimental investigation of the title compound have been reported up to now. We performed the present study to provide experimental and theoretical information concerning the title compound. Therefore, this study aims to give a complete description of the molecular geometry and most stable conformations, molecular vibrations, chemical shifts, electronic transitions and nonlinear optical (NLO) features of the title compound.

2. Experimental procedure

2.1. Synthesis

The title compound, (E)-2-(((4-bromo-2-(trifluoromethoxy)phenyl)imino)methyl)-4-nitrophenol, was prepared by reflux a mixture of a solution containing 2-hydroxy-5-nitrobenzaldehyde (0.0138 g, 0.082 mmol) in 20 ml ethanol and a solution containing 4-bromo-2-(trifluoromethoxy)aniline (0.0211 g, 0.082 mmol) in 20 ml ethanol. The reaction mixture was stirred for 1 hunder reflux. The crystals of suitable for (E)-2-(((4-bromo-2-(trifluoromethoxy)phenyl)imino)methyl)-4-nitrophenol X-ray analysis were obtained from ethyl alcohol by slow evaporation (yield%35; m.p 198–200 °C).

2.2. Materials and measurements

The FT-IR spectra of the title compound using KBr pellet were recorded in the range of 4000–400 cm^{-1} with a Bruker Vertex 80 V FT-IR spectrometer. ^1H and ^{13}C NMR spectra were measured in ethanol solution on spectrometer at VARIAN Infinity Plus 300 and at 75 MHz, respectively. ^1H and ^{13}C chemical shifts are referenced to the internal deuterated solvent. Electronic spectrum was measured using a Unicam UV2 spectrophotometer in ethanol solution in the range from 200 to 600 nm.

2.3. X-ray crystal structure determination

A pale yellow crystal of size 0.55 × 0.43 × 0.20 mm^3 was chosen for the crystallographic study, and then carefully mounted on goniometer of a STOE IPDS II diffractometer. All diffraction measurements were performed at 296 K using monochromated Mo Kα radiation.

2.4. Data collection

Single-crystal X-ray data were collected on a Stoe IPDS II [11] single crystal diffractometer using monochromated Mo Kα radiation at 296 K. X-AREA [11] and X-RED [12] programs were used to cell refinement and data reduction, respectively. SHELXS-97 [13] and SHELXL-97 [13] programs were used to solve and refine the structure, respectively. ORTEP-3 for Windows [14] was used to preparation the figures. WinGX [15] and PLATON [16] software were used to prepare material for publication.

H1 and H5 atoms attached to O atoms were located in difference map and refined freely. All H atoms attached to C atoms were fixed geometrically and treated as riding with C—H = 0.930 Å and $U_{iso}(H) = 1.2\ U_{eq}(C)$. Details of the data collection conditions and parameters of refinement process are given in Table 1.

3. Computational procedure

The molecular modeling and conformational analysis of the title compound were performed by using the Gaussian 09 program [17]. The output files were visualized via GaaussView 5 software [18]. The structural properties and vibration spectra of the title compound were determined through the applications of B3LYP (Becke's three-parameter hybrid model using the Lee–Yang Parr correlation functional) [19,20] and PBE1PBE (generalized-gradient-approximation exchange–correlation functional of Perdew, Burke, and Ernzerhof) [21] with the 6-311++G(d,p) basis set [22]. In order to find out the most stable conformations of the title compound, conformational analyses were carried out by using B3LYP/6-31G level. Moreover, a detailed assignment of vibrational modes for the title compound was performed on the basis of potential energy distribution (PED) by using VEDA 4 program [23] based on the B3LYP level. ^1H NMR and ^{13}C NMR chemical shifts were calculated within GIAO approach [24] which is one of the most common approaches for calculating nuclear magnetic shielding tensors. NBO analysis was performed to display interaction between the 'filled' donor-type NBO and 'empty' acceptor-type NBO in the molecule. The representation of highest occupied molecular orbital (HOMO) and

Table 1
Crystal data and structure refinement for the title compound.

Formula	$C_{14}H_8BrN_2O_4F_3$
Crystal system	Triclinic
Color/shape	Colorless/stick
Temperature	296 K
Space group	*P*−*1*
Unit cell dimensions	
	a = 7.674 (4) Å
	b = 12.584 (6) Å
	c = 15.921 (6) Å
	α = 89.62 (4)°
	β = 84.34(4)°
	γ = 73.77 (4)°
Volume	1468.7(12) $Å^3$
Z	4
Density (calculated)	1.83 Mg m^{-3}
Wavelength	0.71073 Å
Reflections collected	12804
Independent reflections	5673
Absorption coefficient (μ)	2.86 mm^{-1}
Crystal size (mm)	0.6 × 0.27 × 0.03
Absorption correction	Integration X-RED
Data/parameters	5673/441
Goodness-of-fit on F^2	1.00
θ ranges (°)	1.7–26.0
h/*k*/*l*	−9, 9/−15, 15/−19, 19
Final *R* indices [$I > 2\sigma(I)$]	R_1 = 0.047, wR_2 = 0.105
Largest diff. peak and hole	0.36 e $Å^{-3}$, −0.41 e $Å^{-3}$

lowest unoccupied molecular orbital (LUMO) orbital calculations were done at the same levels and basis set. The electronic transitions in the title compound were calculated by using TD-B3LYP and TD-PBE1PBE methods. DFT levels were also used to calculate the dipole moment (μ), the mean polarizability ($\langle\alpha\rangle$), the anisotropy of the polarizability ($\Delta\alpha$), and the total first static hyperpolrizability ($\langle\beta\rangle$). Molecular electrostatic potential (MESP) is calculated by using the B3LYP method. Additionally, thermodynamic properties of the title compound have been calculated by using the quantum chemical methods.

4. Results and discussion

4.1. Description of the crystal structure

The title compound, $C_{14}H_8BrN_2O_4F_3$, consists of 4-bromo-2-(trifluoromethoxy)aniline and 2-methyl-4-nitrophenol groups. The title compound contains two molecules in the asymmetric unit and each of these molecules has two phenyl rings (Fig. 2a). The dihedral angles between phenyl rings for each molecule are 1.65 (21)° for Ring 1 (C1—C6)/Ring 2 (C9—C14), 8.91 (18)° for Ring 3 (C15—C20)/Ring 4 (C23—C28). The rings which belong to molecules display the (E) configuration with respect to C=N bond. The title compound contains Schiff base, and some geometrical parameters which belong to Schiff bases are 1.275 (5) Å for C8—N1, 1.327 (5) Å for C14—O1, 1.277 (5) Å for C22—N3 and 1.344 (5) Å for C28—O5. The aromatic C–C distances for the title compound range from 1.367 (6) Å to 1.427 (5) Å. The bond distances and angles of the title compound are given in Table 2, as compared with the theoretical ones. The imino group is coplanar with the hydroxyphenyl ring, as shown by the C9—C8—C7—N1 torsion angle of 0.282. Additionally, it is well known that Schiff bases may present photochromism depending on the planarity or non-planarity, respectively [25].

In the crystal structure, each molecule of the asymmetric unit has intramolecular O—H···N hydrogen bonds, and D—H, H···A, and D—H···A values are observed as 0.79(6) Å, 1.84(6) Å, and 155 (6)°. Besides, intermolecular C—H···O hydrogen bonds is presented in the crystal structure (Fig. 3). The detailed geometric parameters of these hydrogen bonds are given in Table 3.

4.2. Tautomerism

Tautomerism has been investigated comprehensively due to its role in the determination of molecular properties and their application areas. Tautomerism occurs in the title compound as a consequence of intramolecular proton transfer from oxygen to nitrogen atom. This proton transfer is resulted in two tautomer structures as

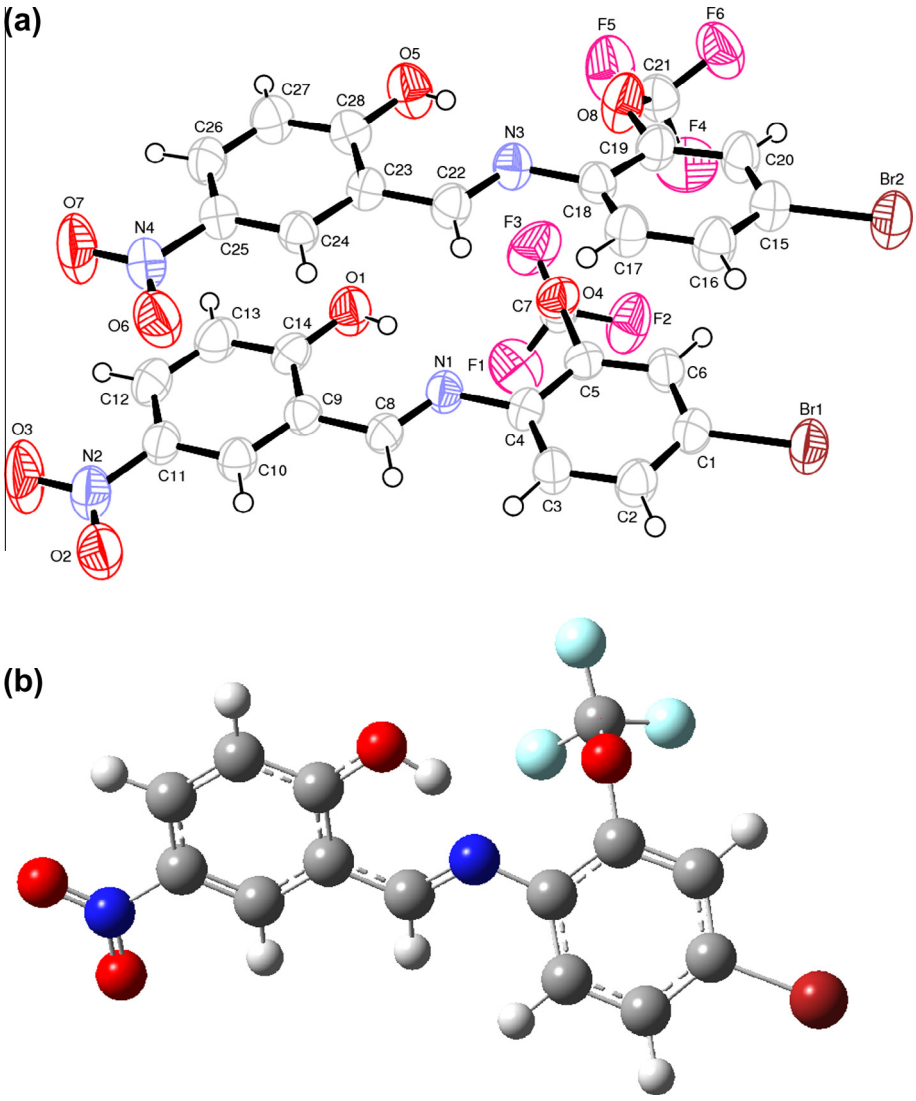

Fig. 2. (a) The molecular structure, showing the atom-numbering scheme, (b) the theoretical geometric structure of the title compound (obtained from B3LYP).

Table 2
Selected experimental and theoretical bond distances and angles of the title compound.

Atoms	Experimental	B3LYP/6-311++G(d,p)	PBE1PBE/6-311++G(d,p)
Bond lengths (Å)			
C1—C2	1.385 (6)	1.391	1.389
C1—C6	1.373 (6)	1.391	1.388
C1—Br1	1.892 (4)	1.910	1.888
C2—C3	1.370 (6)	1.390	1.386
C3—C4	1.385 (5)	1.402	1.397
C4—C5	1.394 (5)	1.403	1.399
C4—N1	1.410 (5)	1.400	1.393
C5—C6	1.374 (6)	1.387	1.383
C5—O4	1.406 (5)	1.400	1.388
C7—F1	1.321 (6)	1.347	1.337
C7—F2	1.326 (5)	1.350	1.339
C7—F3	1.308 (5)	1.329	1.320
C7—O4	1.345 (6)	1.354	1.350
C8—C9	1.451 (5)	1.450	1.444
C8—N1	1.275 (5)	1.286	1.283
C9—C10	1.376 (6)	1.399	1.395
C9—C14	1.427 (5)	1.425	1.421
C10—C11	1.378 (6)	1.383	1.379
C11—C12	1.387 (6)	1.400	1.396
C11—N2	1.456 (6)	1.467	1.458
C12—C13	1.367 (6)	1.380	1.376
C13—C14	1.385 (6)	1.404	1.402
C14—O1	1.327 (5)	1.329	1.320
N2—O2	1.233 (5)	1.227	1.216
N2—O3	1.209 (5)	1.226	1.215
Bond angles (°)			
Br1—C1—C6	119.1(3)	119.291	119.325
C6—C5—O4	119.4 (4)	119.256	119.395
C5—O4—C7	117.5 (3)	118.390	117.517
C5—C4—N1	117.0 (3)	118.995	118.811
C4—N1—C8	122.4 (3)	121.435	121.090
N1—C8—C9	120.6 (4)	121.733	121.373
C9—C14—O1	121.2 (4)	122.024	121.864
C12—C11—N2	119.5 (4)	119.495	119.478
O2—N2—O3	122.2 (4)	124.538	124.813

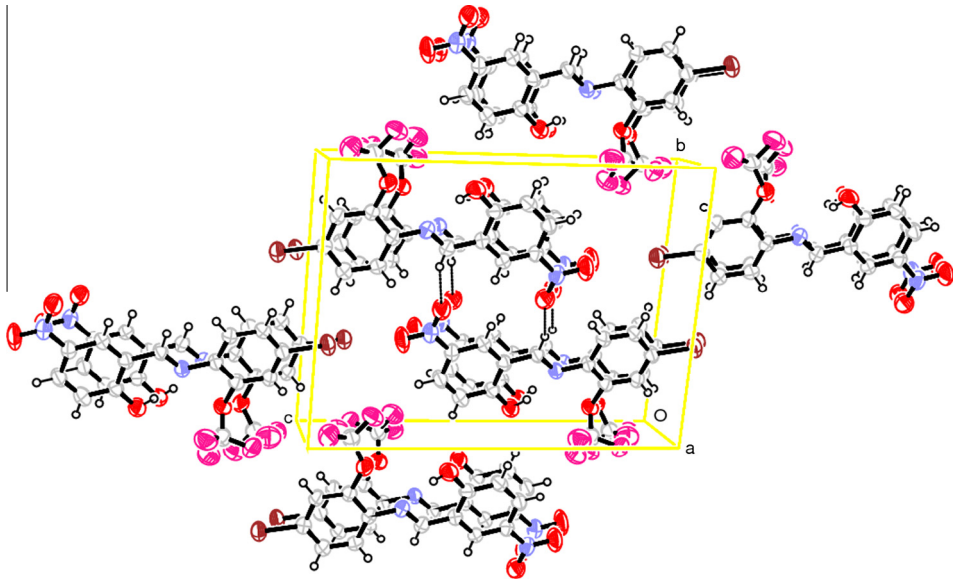

Fig. 3. A view of the packing of the title compound.

enol-imine related to O—H···N type hydrogen bonding and keto-amine related to N—H···O hydrogen bonding in the solid state. The C8—N1 and C14—O1 bond types are important because these bonds are indicator of tautomer form. The double bond between the C8 and N1 atoms indicates that the title compound is in enol-imine form, whereas single bond between these atoms display that the title compound is in keto-amine tautomer form. The C8—N1 [1.275 (5) Å] bond has a double bond character, while the C14—O1 [1.327 (5) Å] bond has a single bond character. As can be seen Fig. 2a,b, H atom bounds to O1, and these atoms along with the N atom form O—H···N hydrogen bonding. Ground state energy of the T1 (enol-imine) is calculated as −3822.64485 Hartree, while

Table 3
Hydrogen-bond geometry for the title compound.

D—H···A	D—H (Å)	H···A (Å)	D···A (Å)	D—H···A (°)
O1—H1···N1	0.79 (6)	1.84 (6)	2.578 (5)	155 (6)
O5—H5···N3	0.74 (5)	1.91 (5)	2.605 (5)	155 (5)
C8—H8···O6^{i}	0.93	2.46	3.309 (5)	153
C22—H22···O2^{i}	0.93	2.49	3.352 (6)	154

T2 (keto-amine) is calculated −3822.63782 Hartree. Considering that the mentioned cases, it is understood that the title compound exists in enol-imine form in the solid state.

4.3. Geometry optimization and conformational analysis

To the best of our knowledge, neither experimental nor theoretical data on the geometrical parameters of the title compound is not available in the literature. The optimized bond lengths and bond angles of the title compound are listed in Table 2. There is slightly difference between the experimental and theoretical parameters due to the fact that the theoretical calculations belong to isolated molecule in gas phase while the experimental results belong to molecule in solid state. Considering that the geometry of the solid state structure is subject to intra and intermolecular interactions, such as hydrogen bonding and van der Waals interactions, it is expected that DFT levels predict slightly greater values than experimental ones.

The C-C bond lengths in the rings vary from 1.380–1.404 Å for B3LYP level and 1.376–1.402 Å for PBE1PBE level. From the bond lengths calculated with B3LYP level, some C—C bond lengths [C1—C2 = 1.391 Å, C1—C6 = 1.391 Å, C2—C3 = 1.390 Å and C5—C6 = 1.387 Å] are lower than other C—C bond lengths [C3—C4 = 1.402 Å and C4—C5 = 1.403 Å]. This deformation of symmetry is due to the various substituents such as —NO_2, —Br and —OH in the rings. When compared with the experimental values, the computed O—H bond length is slightly higher because of the involvement of these bonds in the intramolecular interaction in the crystalline state. The C4—N1—C8 unit combining two rings has an angle of 122.4 (3)°, and this angle is calculated as 121.435° and 121.090° for B3LYP and PBE1PBE levels, respectively. The bond lengths of C8—N1, O2—N2 and O3—N2 reflect the double bond character with the bond lengths of 1.275 (5) Å, 1.233 (5) Å and 1.209 (5) Å. These bond lengths are predicted by the bond lengths of 1.283 Å, 1.216 Å and 1.215 Å for PBE1PBE level. In the optimized structure, the geometry of the hydrogen bond is examined, and it is seen that O1—H1···N1 hydrogen bond that exists between the phenol O1 atom and imine N1 atom, D—H, H···A, and D—H···A values are 0.99 Å, 1.74 Å, and 146° for B3LYP level and 0.99 Å, 1.69 Å, and 147° for PBE1PBE level. The presence of the hydrogen bond appears as an important property of the molecule, stabilizing its conformation in the crystal; as shown in the especially NBO section.

The conformational analysis has been performed to determine the most stable conformer of the title compound by using B3LYP/6-31G level. During the scan, the whole geometrical parameters were simultaneously relaxed, while the N1—C8—C9—C14 dihedral angle was varied in steps of 10° ranging from 0° to 360°. In Fig. 4, it is seen that there are two maximum on the potential energy surfaces, which consist of a local maximum and a global maximum. As can be seen from Fig. 4, the local maximum point is predicted at 90° with the energy value of −3819.32241 Hartree, while the global maximum is predicted at 270° with the energy value of −3819.31815 Hartree. As for the minimum points, two minima which consist of a local minimum at 180° (−3819.33059 Hartree) and a global minimum at 0° (−3819.35103 Hartree) are predicted by using B3LYP/6-31G level.

4.4. IR spectroscopy

The FT-IR spectrum of the title compound was recorded in the frequency region of 4000–400 cm^{-1}, and measured data along with the harmonic vibrational frequencies calculated using B3LYP and PBE1PBE with 6-311++G(d,p) basis set are given in Table 4. Furthermore, the FT-IR and the predicted spectra for the title compound are given in Fig. 5, as compared with the each other. None of the predicted vibrational spectra have any imaginary frequency prove that the optimized geometry is located at the lowest point on the potential energy surface. It is well known that DFT levels systematically overestimate the vibrational wavenumbers. Therefore, the scaling factor values of 0.9899 for B3LYP/6-311++G(d,p) and 0.9800 for PBE1PBE/6-311++G(d,p) were used in order to correct anharmonicity and neglected part of electron correlation [26].

4.4.1. C—H vibrations

C—H stretching vibrations of aromatic and hetero atomic structures generally appear in the range of 3100–3000 cm^{-1} [26]. These modes are not affected by substituent, and so they are pure vibration modes (Table 4). In the FT-IR spectrum of title compound, asymmetric and symmetric C—H stretching vibrations are observed at 3120 and 3042 cm^{-1}. The corresponding bands in the predicted spectra are calculated in the range of 3190–3019 cm^{-1} for B3LYP level and 3177–3012 cm^{-1} for PBE1PBE level. These modes are almost pure modes with the 88–99% contribution of PED. The most prominent and most informative bands in the spectra of aromatic compounds appear in the range of 900–675 cm^{-1} [27]. These bands results from the out-of plane bending of the ring C—H bonds. The C—H in-plane bending vibrations appear at 1482, 1206, 1100 and 1042 cm^{-1}, while the out of plane ones appear in the range of 979, 945, 875 and 837 cm^{-1}. The corresponding bands in predicted spectra are calculated as consistent with the experimental ones. According to PED, these in-plane and out of plane bending vibrations are mixed modes mostly coupled with other bending and stretching modes.

4.4.2. Hydroxyl group vibrations

The vibrations corresponding to the hydroxyl group are the stretching, in-plane and out of plane bending vibrations of C—O and O—H moieties. The O—H group is likely to be most vulnerable to the environment; hence they show an exact shift in the spectra of the hydrogen-bonded species. The nonhydrogen-bonded or a free hydroxyl group absorb strongly in the 3550–3700 cm^{-1} region [28]. If the intramolecular hydrogen bonding occurs in six membered ring systems, the O—H stretching band would be reduced to 3200–3550 cm^{-1} region [29]. In this study, the O—H stretching vibration appears at 3416 cm^{-1} in FT-IR spectrum, while this band is assigned at 3162 cm^{-1} for B3LYP level and 3140 cm^{-1} for PBE1PBE level with the 89% contribution of PED. In-plane O—H bending modes is observed at 1542 and 1408 cm^{-1}, while the corresponding bands are calculated at the range of 1654–1426 cm^{-1} for B3LYP and 1674–1434 cm^{-1} for PBE1PBE. The bands observed at 837 cm^{-1} is assigned as out-of plane bending of O—H group, and this band is calculated at 865 and 842 cm^{-1} for B3LYP with the 62% and 27% contribution of PED, respectively.

4.4.3. Phenyl ring vibrations

The ring C=C vibrations generally appear 1625–1430 cm^{-1} for aromatic systems [30]. The bands at 1622, 1592, 1587, 1571, 1408, 1308 and 1042 cm^{-1} are assigned as the C—C vibrations which are calculated at the range of 1654–1079 cm^{-1} and 1674–1081 cm^{-1} for B3LYP and PBE1PBE level, respectively. These vibration modes are highly mixed modes with the range of 55–11% contribution of PED, and they are mostly coupled with the NC, NO and FC stretching vibrations as well as some bending vibrations. Peaks

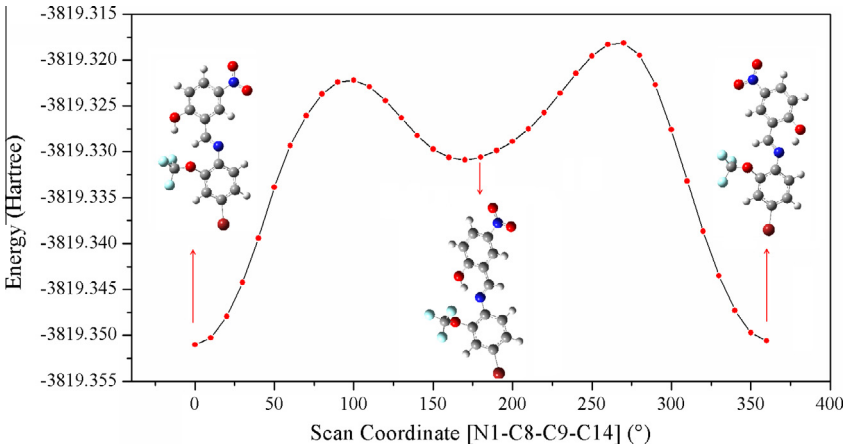

Fig. 4. One-dimensional potential energy surface (PES) scan of the calculated energies vs. τ(N1—C8—C9—C14) dihedral angle of the title compound.

at 1571, 917, 771, 701 and 643 cm^{-1} are designated as C—C—C in plane bending vibrations. According to the PED, these modes are predicted at the range of 1583–638 cm^{-1} with 35–10% contributions of PED. The out of plane C—C—C—C bending vibrations are observed at 979 and 481 cm^{-1} in the FT-IR. Predicted wavenumbers of these modes are consistent with the experimental ones.

4.4.4. Nitro group vibrations

In aromatic nitro compounds, symmetric and asymmetric stretching vibrations of NO_2 group give peaks at the range of 1570–1485 cm^{-1} and 1370–1320 cm^{-1} [31] respectively. In FT-IR spectrum, the bands at 1587, 1542, 1340 and 1308 cm^{-1} are assigned as N—O stretching vibrations. Additionally, these modes are calculated at the range of 1596–1351 cm^{-1} and 1623–1355 cm^{-1} for B3LYP and PBE1PBE, respectively. These vibration modes coupled with some C—C and N—C stretching modes with the range of 15–55% contribution of PED. The O—N—O in plane bending vibration is calculated at 839 and 840 cm^{-1} for B3LYP and PBE1PBE levels, respectively. This band also appears at 643 cm^{-1} which is calculated at 647 and 643 cm^{-1}, respectively.

4.4.5. N—C, C—Br, C—F and C—O vibrations

The C=N stretching vibration is responsible for the peaks at 1622 and 1582 cm^{-1} in FT-IR spectrum. The corresponding peaks in the predicted spectra are assigned at 1654 and 1596 cm^{-1} with 15% and 11% contributions of PED, respectively. The band at 1266 cm^{-1} is designated as C—N stretching vibration, and this mode is assigned at 1274 and 1279 cm^{-1} for B3LYP and PBE1PBE levels, respectively. The in-plane N—C—C bending peak is observed at 574 cm^{-1}, while it is calculated at 567 cm^{-1} with 14% contribution of PED. In the FT-IR spectrum of the title compound, the band at 643 cm^{-1} is assigned to the C—Br stretching vibration. The peak at 647 cm^{-1} predicted with the PED exactly correlates with experimental observation. The bands at 1237, 1206, 1186, 1157 and 917 cm^{-1} in FT-IR spectrum are appointed as F—C stretching modes, and these modes are calculated in the range of 1252–602 cm^{-1} and 1273–607 cm^{-1} as mostly coupled modes. In the predicted spectra, in-plane F—C—F bending vibration is appointed at 667 and 669 cm^{-1} for B3LYP and PBE1PBE levels, respectively. The C—O stretching vibration is responsible for the peaks at 1237, 1186 and 771 cm^{-1} in the FT-IR spectrum. These bands are observed at the range of 1292–785 cm^{-1} for B3LYP level and 1315–788 cm^{-1} for PBE1PBE level. These modes are mostly coupled by some stretching and bending vibrations with the range 10–41% contributions of PED. In plane O—C—C bending vibration is assigned at 630 cm^{-1} for both levels of theory with 11% contribution of PED.

4.5. NMR spectroscopy

NMR spectroscopy is currently used to determination of biological macromolecules. Chemical shifts are considered as an imperative part of the information contained in NMR spectra. The combined use of NMR and computer simulation methods offers a powerful way to interpret and predict the structure of large biomolecules [32]. ^{13}C and ^{1}H spectrum for the title compound has been recorded in ethanol solution.

The gauge invariant atomic orbital (GIAO) ^{13}C and ^{1}H chemical shift values (with respect to TMS) were compared to the experimental ^{13}C and ^{1}H chemical shift values in Table 5. The ^{1}H and ^{13}C chemical shift values of TMS were used as 31.9713 and 184.102 ppm [33] by B3LYP/6-311++G(d,p) level. Morever, TMS values for PBE1PBE/6-311++G(d,p) level were calculated as 31.8016 and 188.972 ppm, respectively. It was reported that aromatic carbons give signals in the range of 100–150 ppm [34,35]. In the present study, the chemical shift values of aromatic carbons except that the C14 atom are observed in the range of 141.70–119.22 ppm, while these carbon atoms give peaks at the range of 151.095–123.623 ppm for B3LYP level and 148.050–122.477 ppm for PBE1PBE level. The more electronegativity properties of oxygen and nitrogen atoms polarize the electron distribution in its bond to adjacent carbon atom and decrease the chemical shifts value. So, the chemical shift values of C14, C5 and C8 atom are higher than the others. A signal at the 189.72 ppm in FT-NMR indicates the presence of carbonyl group in the title compound. This peak theoretically appeared at 175.752 and 172.988 ppm for B3LYP and PBE1PBE levels, respectively.

In the ^{1}H NMR spectrum, the signal at 10.27 ppm is assigned to the H1 atom bounding to O5 atom. The corresponding signals in predicted spectra are designated at 13.010 and 13.985 ppm for B3LYP and PBE1PBE level, respectively. This peak is observed in down field due to the electronegativity of oxygen atom [36]. H8 atom which gives signal at 8.68 ppm is responsible for the peaks appearing at higher chemical shift of 8.326 and 8.694 ppm for B3LYP and PBE1PBE levels, respectively. The six aromatic protons of phenyl rings are observed in the range of 8.67–7.18 ppm, while these peaks are calculated at the range of 8.316–6.835 for B3LYP level and 8.668–7.246 ppm for PBE1PBE level.

4.6. Frontier molecular orbitals (FMOs)

FMOs play an important role in the optical and electronic properties, as well as UV–vis spectrum and chemical reactions. The HOMO is the orbital that acts as an electron donor, whereas LUMO is an orbital that acts as electron acceptor. The energy gap between

Table 4
Comparison of the FT-IR and the predicted vibration frequencies for the title compound.

Assignments with B3LYP (PED%)[a]	Experimental	Theoretical					
		PBE1PBE/6-311++G(d,p)			B3LYP/6-311++G(d,p)		
		Scaled freq.[b]	I_{IR}[c]	I_R[d]	Scaled freq.[b]	I_{IR}[c]	I_R[d]
ν (CH) 99	3120	3177	2.29	83.10	3190	1.75	84.93
ν (CH) 91	–	3176	6.46.	150.13	3189	6.21	137,24
ν (CH) 96	–	3164	0.01	109.99	3173	1.14	121,50
ν (CH) 99	–	3160	2.75	105.89	3172	5.46	43.51
ν (CH) 83	3042	3157	3.59	9.36	3168	74.85	130.24
ν (OH) 89	3416	3140	2.17	29.15	3162	589.43	159.05
ν (CH) 99	2924	3084	751.89	196.68	3150	1.28	31.34
ν (CH) 99	2853	3012	48.98	48.68	3019	32.28	47.65
ν (NC) 42 + ν(CC) 12	1622	1674	95.16	1383.12	1654	84.65	1161.27
ν (NC) 15 + ν(CC) 18	–	1668	631.87	1184.85	1649	503.24	1103.55
ν(CC) 23	1592	1639	193.16	332.30	1606	42.33	1379.37
ν (NC) 11 + ν(ON) 15 + ν(CC) 11	1587	1623	33.04	1785.85	1596	171.25	1705.88
ν(CC) 45 + β(CCC) 10	1571	1603	2.45	413.55	1583	15.34	43.47
ν (ON) 55 + β(HOC) 14	1542	1599	15.25	1140.13	1576	24.99	536.16
β(HOC) 14	1526	1512	54.69	110.13	1503	61.89	134.74
β(HCC) 24	1482	1499	209.35	739.69	1492	205.79	589.81
ν(CC) 13 + β(HOC) 12	–	1481	14.59	216.26	1472	0.93	571.10
ν(CC) 41 + β(HOC) 22	1408	1434	10.09	37.55	1426	22.73	34,26
ν(CC) 53 + β(HCC) 22	–	1420	21.56	49.05	1413	15.23	46,45
β(HCN) 49	1366	1400	643.77	508.57	1372	14.55	16,33
ν (ON) 36 + ν(CC) 11	1340	1378	31.97	333.11	1355	335.19	106,09
ν (ON) 36 + ν(CC) 13	1308	1355	57.82	168.51	1351	265.75	876.18
ν(CC) 33 + β(HCC) 41	–	1328	53.82	93.53	1316	94.53	72.51
ν(CC) 53 + ν(OC) 41	–	1315	1.27	62.47	1292	0.10	15.74
ν(NC) 13 + β(HCC) 58	1266	1279	93.33	333.57	1274	20.04	255.51
ν(OC) 11 + ν(FC) 39 + ω(FOFC) 11	1237	1273	563.15	5.24	1252	527.46	6.15
ν(FC) 10 + β(HCC) 39 + β(HCN) 10	1206	1242	16.04	74.240	1248	109.81	47.16
β(HCC) 34	–	1231	14.20	496.50	1235	47.10	329.57
ν(CC) 24 + ν(OC) 18	–	1227	84.46	71.11	1214	43.10	457.33
ν(OC) 35 + ν(FC) 15	1186	1220	390.65	4.86	1199	331.27	15.56
ν(OC) 16 + ν(OC) 12 + β(HCC) 14	–	1194	122.69	140.74	1187	241.66	101.79
ν(FC) 77 + τ(FOFC) 19	1157	1181	347.65	4.26	1146	345.10	2.97
ν(CC) 27 + β(HCC) 54	1100	1127	22.37	75.41	1133	17.85	36.57
β(HCC) 34	1087	1122	18.37	26.11	1132	41.07	75.28
ν(CC) 35 + β(HCC) 43	–	1099	166.32	17.96	1096	147.49	21.20
ν(CC) 55 + β(HCC) 21	1042	1081	10.10	98.67	1079	12.63	104.61
τ(HCNC) 79	–	990	9.11	67.45	994	8.14	76.73
τ(HCCC) 77 + τ(CCCC) 15	979	977	1.77	7.28	983	0.93	4.18
τ(HCCC) 56	945	952	23.33	38.60	954	11.15	29.54
τ(HCCC) 29	–	946	21.19	11.26	948	34.53	26.52
ν(FC) 10 + β(CCC) 35	917	939	25.82	13.65	932	24.88	22.00
τ(HCCN) 77	903	923	15.07	6.43	929	11.12	7.31
τ(HCCC) 47	875	889	48.62	1.34	888	2.17	3.32
β(CCN) 12 + τ(HCCC) 21	–	885	5.26	4.71	880	26.52	3.56
τ(HOCC) 62 + τ(HCCC) 11	–	877	17.34	3.58	865	26.75	1.93
τ(HOCC) 27 + τ(HCCC) 51	837	848	14.03	4.35	842	79.33	1,27
β(ONO) 28	-	840	43.25	0.25	839	10.40	3.21
τ(HCCC) 57	817	827	17.72	2.40	825	17.96	9.09
ν(OC) 10 + β(CCC) 21	771	788	2.36	36.51	785	2.34	30.89
ω(OCCC) 14 + ω(NCCC) 20	752	754	9.93	2.14	752	10.76	2.03
ω (OCON) 50 + ω(OCCC) 17 + ω(NCCC) 11	–	745	18.26	1.00	737	13.33	1.19
τ(HCCC) 19 + ω (OCON) 35 + ω(OCCC) 19	–	725	1.77	1.47	726	10.01	2.75
β(CCC) 16 + β(CCN) 10	701	700	37.86	9.46	700	35.79	8.87
ν(FC) 12 + β(FCF) 11 + τ(CCCC) 26	–	669	2.94	11.27	667	1.54	12.89
ν(BrC) 32 + β(CCC) 16 + β(ONO) 12	643	646	13.07	6.41	647	13.38	3.90
β(CCC) 22 + τ(FOFC) 12	–	638	4.23	1.99	638	5.38	4.20
β(OCC) 11 + ω (FOFC) 11	–	630	3.99	4.14	630	1.52	5.84
ν(FC) 12 + ω (FOFC) 35	–	607	9.08	4.09	602	9.26	3.78
τ(HCCC) 10 + τ(CCCC) 38 + ω(BrCC) 11	–	571	9.25	2.24	572	10.29	2.00
β(NCC) 14	574	567	3.83	2.75	567	3.46	2.95
β(ONC) 20 + τ(CCCC) 11	–	541	5.51	5.94	542	4.73	7.95
β(ONC) 23	538	535	0.76	3.37	535	1.98	0.95
β(FCF) 18	517	511	5.55	6.88	510	5.08	13.52
β(FCF) 14 + τ(CCCC) 11	481	485	4.53	44.03	485	3.11	35.87
τ(CCCC) 16	–	458	0.08	3.33	459	2.20	13.42
β(FCF) 33	–	451	1.24	3.77	452	2.53	3.48
β(OCC) 38	–	447	4.35	4.09	447	2.06	0.45

ν: stretching, β: bending, τ: out-of plane bending; ω:torsion.
[a] Vibrational modes are based on potential energy distribution (PED) and only contributions over 10% are given.
[b] Scaled frequencies are in unit of cm^{-1}.
[c] I_{IR} infrared inten. are in unit of km mol^{-1}.
[d] I_R Raman activ. are in unit of $Å^4$ amu^{-1}.

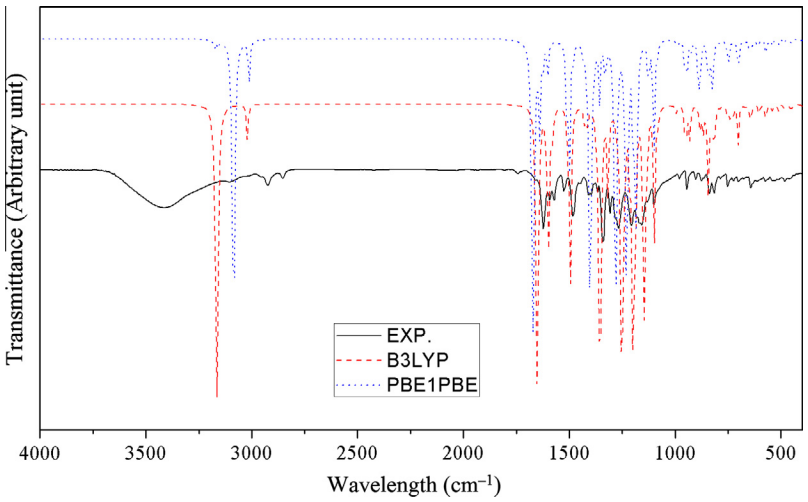

Fig. 5. Experimental and theoretical IR spectra of the title compound.

Table 5
Theoretical and experimental ^{13}C and ^{1}H isotropic chemical shifts (with respect to TMS, all values in ppm) of the title compound.

Atom	Experimental	Theoretical	
		B3LYP/6-311++G(d,p)	PBE1PBE/6-311++G(d,p)
^{1}H			
H1	10.27	13.010	13.985
H2	7.79	7.381	7.765
H3	7.18	6.835	7.246
H6	7.63	7.395	7.772
H8	8.68	8.326	8.694
H10	8.67	8.316	8.668
H12	7.79	8.318	8.671
H13	7.24	6.983	7.332
^{13}C			
C1	140.30	147.821	143.164
C2	135.18	138.763	137.484
C3	122.87	125.001	124.035
C4	140.87	150.545	147.721
C5	141.70	151.095	148.05
C6	129.73	135.097	134.183
C7	128.67	131.967	126.703
C8	166.54	168.595	168.265
C9	120.72	124.222	121.018
C10	131.43	136.092	134.953
C11	140.37	148.757	144.308
C12	132.84	136.965	136.221
C13	119.22	123.623	122.477
C14	189.72	175.752	172.988

the HOMO and LUMO characterizes the molecular chemical stability, chemical reactivity and hardness, softness of the molecule. From Fig. 6, HOMO and LUMO energies are calculated as −7.7672 and −5.4700 eV for B3LYP level and −7.7650 and −5.4781 eV for PBE1PBE level, respectively. The energy gap between the HOMO and LUMO orbital is predicted as 2.2902 and 2.2869 eV, respectively. It is well known that the more HOMO–LUMO energy gap is low, the more charge transportation is prospective. So, these low HOMO–LUMO energy gaps show that the charge transfer occurs in the title compound.

Electronegativity (χ) and chemical hardness (η) can be calculated as used the frontier molecular orbital energies [37,38]. In molecules, electron will be transferred from the one of low χ to that of high χ (electrons flow from high chemical potential to low chemical potential). In title compound, χ values are defined as 1.1451 and 1.1436 eV for B3LYP and PBE1PBE levels, respectively. From the HOMO and LUMO energies, the η values are

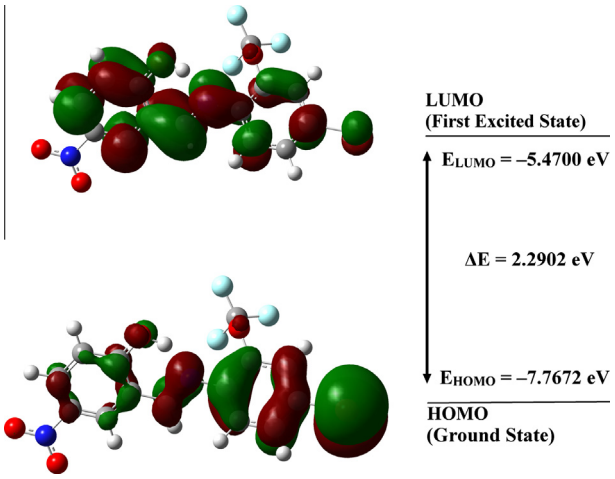

Fig. 6. The frontier molecular orbital with the energies of the title compound.

defined as 6.6186 and 6.6216 eV for B3LYP and PBE1PBE levels, respectively.

In the title compound, HOMO orbitals are localized on mainly hydroxyphenyl ring (44%), 4-bromophenyl (42%) with contributions of Br atom (9%) and imino group (5%), while LUMO orbitals are localized on hydroxyphenyl ring (48%), 4-bromophenyl (37%) with contributions of imino group (13%). Accordingly, it can be clearly seen that charge transfer occurs from Br atom to remain part of the title compound. The imino group plays a relatively significant role in the HOMO−1 (8%), LUMO+6 (22%) and LUMO+5 (20%). As for the nitro group (—NO2) play essential role in the LUMO+1 (45%) and HOMO−7 (50%). Hydroxyl and trifluoromethoxy substituent does not play an important role in the formations of the molecular orbitals.

The UV–vis spectra of the title compound are given in Fig. 7. Major contributions to the electronic transitions are designated with the aid of SWİZARD program, and obtained results are given in Table 6. The UV–vis spectrum of Schiff bases that exist as enol-imine form indicate the presence of a band at <400 nm, whereas compounds existing in the keto-amine form display a new band, especially in polar and nonpolar solvents, at >400 nm [39]. It can be understood from this case that the title compound exists in the enol-imine form. From Table 6, the absorption band observed at 337 nm is mainly designated by the transitions from

hydroxyphenyl ring (44%), 4-bromophenyl (42%), Br atom (9%) and imino group (5%) to hydroxyphenyl ring (48%), 4-bromophenyl (37%) and imino group (13%). This peak is calculated at 344 and 333 nm for B3LYP and PBE1PBE level, and formed with the contribution of H → L (69%) and H → L+1 (26%) transitions. The absorption bands at the longer wave lengths 337 and 306 nm of the title compound are caused by the n → π^* transition. The absorption band at the range of 267–206 nm is caused by $\pi \rightarrow \pi^*$ transitions. The λ_{max} is a function of substitution, the stronger donor character of the substitution, the more electrons pushed into the molecules, the larger λ_{max}. These values may be slightly shifted by solvent effects. The roles of substituents and the solvents influence on the UV-spectrum. According to B3LYP calculations, these transitions are formed with the contributions of different modes. For example, the electron transition observed at 241 nm is calculated 294 nm for B3LYP level and 276 for PBE1PBE level, and this band is mainly formed by two electronic transition modes [HOMO−1 → LUMO+1 (87%) and HOMO−1 → LUMO (7%)], while the transition peak observed at 221 nm is calculated at 269 for B3LYP and 261 nm for PBE1PBE level, and it is formed with the contributions of H−3 → L+1 (37%), H−6 → L (34%) and H−2 → L (9%).

4.7. Molecular surfaces

The color scheme for the MESP surface is as follows: red for electron rich, partially negative charge; blue for electron deficient, partially positive charge; light blue for slightly electron deficient region; yellow for slightly electron rich region; green for neutral; respectively [40]. In other words, electrostatic potential increases in the order red < orange < yellow < green < blue. The color code of these maps is in the range between −0.0771 a.u (deepest red) to 0.0771 a.u (deepest blue) in title complex. The negative regions of MEP are related to electrophilic reactivity and the positive ones are related to nucleophilic reactivity. It is clear from Fig. 8 that this molecule has several possible sites for electrophilic attack including O1 atom of hydroxyl group, O2 and O3 atoms of nitrobenzene group as well as O4, Br1 and F atoms. The most negative $V(r)$ values are −0.072 for O2 and O3 atom. However, positive regions are localized N1, N2, C8 and all of the hydrogen atoms.

From Fig. 8, the negative region is mainly localized on the hydroxyl and nitro group oxygen atoms, O1, O2 and O3. It can be seen from Fig. 8, the negative ESP is localized more over the O1 atom. Additionally, a relatively positive region is over N1 and C8—H bonds. Therefore, Fig. 8 confirms the existence of intramolecular O—H···N interactions observed in the solid state. The predominance of light green region in the MESP surfaces corresponds to a potential halfway between the two extremes red and dark blue color.

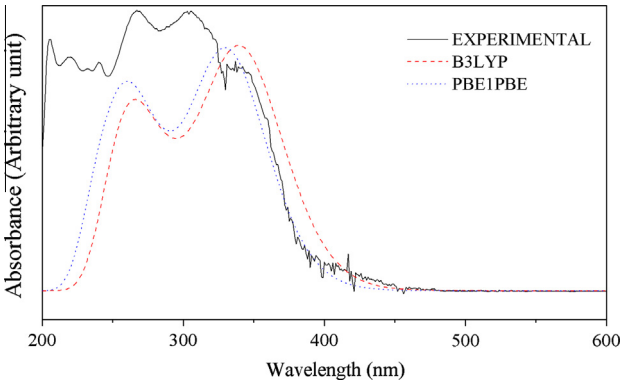

Fig. 7. The experimental and theoretical UV–vis spectra of the title compound.

4.8. Natural bond orbital (NBO) analysis

NBO analysis have been performed for the title compound at the DFT/B3LYP/6-311++G(d,p) level in order to elucidate the intramolecular, hybridization and delocalization of electron density within the molecule. The natural bond orbital analysis provides an efficient method for investigating intra- and intermolecular bonding and interaction among bonds, and also provides a reliable basis for investigating charge transfer or conjugative interactions in molecular systems [41]. According to NBO calculations, the electronic configuration of Br1 atom is [core]$4S^{1.86}4p^{5.03}4d^{0.01}5p^{0.01}$ with 27.999 core electrons, 6.889 valance electrons, 0.019 Rydberg electrons. In total, this configuration gives 34.908 electrons which are consistent with the natural charge [0.092] on the Br1 atom.

NBO analysis provides an effective method for investigating intra- and intermolecular bonding and interaction among bonds, and also gives a practical basis for investigating charge-transfer or conjugative interaction in a molecular systems. The intramolecular hyperconjugative interaction are formed by the orbital overlap between bonding π (C3—C4) and antibonding π^* (C5—C6) and π^* (C1—C2) orbitals. The interaction energies of π (C3—C4) → π^* (C5—C6) and π (C3—C4) → π^* (C1—C2) are calculated as 20.45 and 22.05 kcal/mol, respectively. These interactions result in intramolecular charge transfer causing stabilization of the title compound. The same kind interactions are observed between the bonding π (C5—C6) and antibonding π^* (C3—C4) and π^* (C1—C2) orbitals. As can be seen from Table 7, these interactions are observed as increase in electron density (ED) in antibonding orbital that weakens the respective bonds. The LP(3) O2 → π^*(N2—O3), LP(2) O3 → σ^*(N2—O2) and LP(2) Br1 → π^* (C1—C2) interaction energies are 160.62, 19.03 and 10.18 kcal/mol, respectively. These energies are clearly evidence for the elongation and weaken of the O2—N2, O3—N2 and Br1—C1 bonds, and also show the hyperconjugation interaction between the electron donating groups to the acceptor groups in the title compound.

NBO analysis clearly explains the evidence of the formation of H-bonded interaction between the LP(N) and σ(O—H) antibonding orbitals. The stabilization energies $E(2)$ associated with hyperconjugative interaction LP(1) N1 → σ^*(O1—H1), is equal to 23.46 kcal/mol, which quantify the extend of intramolecular hydrogen bonding (Table 7). Thus it is apparent that O—H···N interaction substantially affect the crystal packing of this compound.

4.9. Energies and dipole moments

Dipole moment in a molecule is an important property since it can be used as an indicator of the charge movement across the molecule. The direction of the dipole moment depends on the positive and negative charge centers. The dipole moment of the title compound is calculated as 3.5560 and 3.5330 Debye for B3LYP and PBE1PBE levels, respectively. From Table 8, maximum contribution to the dipole moment is from x direction, whereas contribution of z direction to the dipole moment is negligible.

It is well known that the higher values of the dipole moment (μ), the molecular polarizability (α), and the hyperpolarizability (β) are important for more active NLO properties. Importance of the polarizability and first the hyperpolarizability of molecular systems derive from the efficiency of electronic communication between acceptor and donor groups which have a vital role in determining the intra molecular charge. The coplanar of phenyl-nitro group and stronger accepted property of the nitro groups should increase the β value of a compound. Also, donor character of the hydroxyl group contributes to increase of the β values.

The calculated α values are equal 34.192×10^{-24} for B3LYP level and 33.551×10^{-24} esu for PBE1PBE level. These α values are approximately 1.5 times greater than that of *para*-Nitro-Aniline

Table 6
Theoretical and experimental electronic transitions, oscillator strength and major contributions for the title compound.

Experimental λ (nm)	Osc. strength	Theoretical						
		B3LYP/6-311++G(d,p)		PBE1PBE/6-311++G(d,p)		Major contributions with B3LYP		
		λ (nm)	Osc. strength	λ (nm)	Osc. strength			
337	0.6671	344	0.5661	333	0.5795	H → L (69%)	H → L+1 (26%)	
306	0.8154	331	0.0187	–	–	H → L+1 (55%)	H → L (25%)	H−1 → L (17%)
267	0.8275	309	0.0877	295	0.1550	H−1 → L (66%)	H → L+1 (16%)	H−1 → L+1 (9%)
241	0.6738	294	0.1442	276	0.1120	H−1 → L+1 (87%)	H−1 → L (7%)	
221	0.6840	269	0.2776	261	0.3504	H−3 → L+1 (37%)	H−6 → L (34%)	H−2 → L (9%)
206	0.7320	252	0.1478	240	0.1431	H−6 → L (27%)	H−3 → L (20%)	H−3 → L+1 (16%)

H: HOMO; L: LUMO.

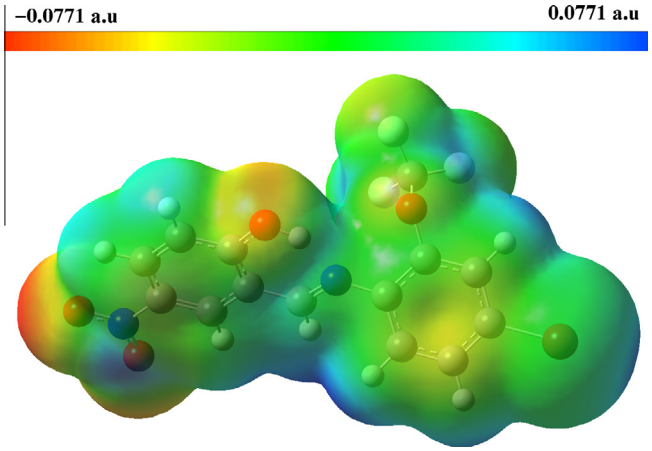

Fig. 8. Total electron density mapped with electrostatic potential surface of the title compound.

(*p*NA) molecule which is a typical NLO material [42,43]. *p*NA molecule was chosen as a reference molecule because there were no experimental values about the title complex in the literature. The β values are calculated as 18.819×10^{-30} and 16.925×10^{-30} esu for B3LYP and PBE1PBE levels, respectively. When our results are compared to that of *p*NA, it can be said that title compound displays significant polarizability and first hperpolarizability properties, and it can be used as an effective NLO material.

4.10. Thermodynamic parameters

The standard statistical thermodynamic functions: heat capacity ($C^0_{p,m}$), entropy (S^0_m), and enthalpy changes (H^0_m) for the title compound were calculated on the basis of vibrational analysis at B3LYP and PBE1PBE levels with the 6-311++G(d,p) basis set. The statistical thermo chemical analysis of the title compound is carried out considering the molecule to be at 298.15 K and one atmospheric pressure, and obtained data is given in Table S1 in supplementary information. It is well known that the total energy

Table 7
Second-order perturbation theory analysis of Fock matrix on NBO basis for the title compound (obtained from B3LYP/6-311++G(d,p) level).

Donor	Type	ED(i) (e)	Acceptor	Type	ED(i) (e)	$E(2)$[a] (kcal/mol)	$E(j)$–$E(i)$[b] (a.u.)	$F(i,j)$[c] (a.u.)
C9—C10	π	1.64248	C8—N1	π*	0.19442	24.30	0.27	0.075
C8—N1	π	1.91331	C9—C10	π*	0.38241	7.33	0.36	0.050
C4—C3	σ	1.96996	C4—C5	σ*	0.03674	3.82	1.25	0.062
C4—C3	σ	1.96996	C3—C2	σ*	0.01561	2.89	1.29	0.055
C4—C3	π	1.63339	C5—C6	π*	0.35346	20.45	0.28	0.068
C4—C3	π	1.63339	C2—C1	π*	0.38916	22.05	0.28	0.070
C5—C6	σ	1.96980	C4—C5	σ*	0.03674	4.09	1.27	0.064
C5—C6	σ	1.96980	C6—C1	σ*	0.02519	3.91	1.29	0.063
C5—C6	π	1.68625	C4—C3	π*	0.38707	19.36	0.29	0.069
C5—C6	π	1.68625	C2—C1	π*	0.38916	18.17	0.29	0.066
C2—C1	π	1.66760	C4—C5	π*	0.03674	18.54	0.29	0.066
C2—C1	π	1.66760	C5—C6	π*	0.35346	21.18	0.29	0.070
LP(1) N1		1.85147	C9—C8	σ*	0.02719	3.01	0.84	0.046
LP(1) N1		1.85147	O1—H1	σ*	0.06242	23.46	0.77	0.123
LP(1) N1		1.85147	C8—H8	σ*	0.03618	11.38	0.75	0.085
LP(1) N1		1.85147	C4—C5	σ*	0.03674	1.05	0.91	0.028
LP(2) Br1		1.97493	C2—C1	π*	0.38916	10.18	0.30	0.054
LP(2) O3		1.89991	C5—N2	σ*	0.10140	11.97	0.57	0.074
LP(2) O3		1.89991	N2—O2	σ*	0.05515	19.03	0.72	0.106
LP(2) O2		1.89982	C5—N2	σ*	0.10140	11.95	0.57	0.074
LP(2) O2		1.89982	N2—O3	σ*	0.63291	18.92	0.72	0.106
LP(2) O1		1.88872	C7—F1	σ*	0.12027	13.78	0.57	0.079
LP(2) O1		1.88872	C7—F2	σ*	0.12462	14.15	0.56	0.080
LP(3) O26		1.46053	N2—O3	π*	0.05515	160.62	0.14	0.138
LP(1) C11		1.11416	C9—C10	π*	0.38707	81.50	0.15	0.115
C8—N1	π*	0.19442	C9—C10	π*	0.38241	142.83	0.01	0.067
C8—N1	π*	0.19442	C4—C3	π*	0.38707	78.17	0.01	0.051

ED = electron density.
[a] $E(2)$ means energy of hyperconjugative interactions (stabilization energy).
[b] Energy difference between donor and acceptor i and j NBO orbitals.
[c] $F(i,j)$ is the Fock matrix element between i and j NBO orbitals.

Table 8
Total static dipol moment (μ, in Debye), the mean polarizability ($\langle\alpha\rangle$, in 10^{-24} esu), the anisotropy of the polarizability ($\Delta\alpha$, in 10^{-24} esu), the mean first-order hyperpolarizability ($\langle\beta\rangle$, in 10^{-30} esu) for the title compound.

Property	B3LYP/6-311++G(d,p)	PBE1PBE/6-311++G(d,p)
μ_x	−3.1446	−3.1839
μ_y	−0.9067	−0.8601
μ_z	−1.3910	−1.2670
μ	3.5560	3.5330
μ	2.44 Debye [a]	
α_{xx}	58.682	57.336
α_{yy}	27.137	26.781
α_{zz}	16.756	16.536
$\langle\alpha\rangle$	34.192	33.551
$\Delta\alpha$	22.306	21.606
$\langle\alpha\rangle$	22 $\times10^{-24}$ cm^3 [b]	
β_x	17.311	15.489
β_y	−5.465	−5.136
β_z	4.960	4.490
$\langle\beta\rangle$	18.819	16.925
$\langle\beta\rangle$	15.5 $\times10^{-30}$ esu [c]	

[a] Taken from Refs. [43,44].
[b] Taken from Refs. [43,44].
[c] Taken from Refs. [43,44].

of a molecule is the sum of vibrational, translational, rotational and electronic energies. From Table S1, there is only small difference between the results obtained from both methods. Therefore, there is an agreement between the B3LYP and PBE1PBE levels for the thermodynamic properties (Table S1). All the thermodynamic data provide information for the further study on the title compound. They can be used to predict the other thermodynamic parameters according to relationships of thermodynamic functions and to determine the directions of chemical reactions according to the second law of thermodynamics [44].

5. Conclusion

In this paper, as well as giving structural, spectroscopic and electronic information concerning the title compound for the first time, this study also prepares the ground for the future investigations. Considering that experimental and theoretical studies are performed in different phase, it can be said that there is a good agreement between the experimental and theoretical data.

- From the optimization of the title compound, it is observed that there are two tautomeric structure of the title compound. Additionally, T1 (enol-imine form) has lower total energy than T2 (keto-amine form) Thus, the title compound exists in enol-imine form in the solid state.
- In FT-IR studies, the O—H stretching vibration shifts from the range of 3550–3700 cm^{-1} to 3416 cm^{-1}, indicating the intramolecular O—H···N hydrogen bonding interaction. The signal at 10.27 ppm in FT-NMR spectrum displays the presence of carbonyl group in title compound, while the peaks in the range of 8.67–7.18 ppm demonstrate the presence of aromatic rings.
- Frontier molecular orbital energies are calculated using B3LYP and PBE1PBE level, and obtained small HOMO–LUMO energies show that charge transfer occurs in the title compound. In any two molecules, electron is transferred from the one of low χ to that of high χ. The low χ values also indicate the presence of the charge transfer.
- From MEP of the title compound, the negative region is mainly localized on the hydroxyl group, while positive region is over N1. Accordingly, the MEP confirms the existence of intramolecular O—H···N interactions observed in the solid state.
- In NBO analysis, The intramolecular hyperconjugative interaction energies [π (C3—C4) → π^* (C5—C6) and π (C3—C4) → π^* (C1—C2)] for the title compound are evidence of the intramolecular charge transfer causing stabilization of the title compound. The stabilization energies $E(2)$ associated with hyperconjugative interaction LP(1) N1 → σ^*(O1—H1), is equal to 23.46 kcal/mol, indicating the extend of intramolecular hydrogen bonding.
- Due to the coplanar structure of phenyl-nitro group, stronger accepted property of the nitro groups and donor character of the hydroxyl group, the title compound displays significant polarizability and first hperpolarizability properties, and it can be used as an effective NLO material.

Acknowledgements

The authors thank the Ondokuz Mayıs University Research Fund for financial support of the project. Crystallographic data (excluding structure factors) for the structure in this paper have been deposited with the Cambridge Crystallographic Data Centre as the supplementary publication no CCDC 937131 for compound. Copies of the data can be obtained, free of charge, on application to CCDC, 12 Union Road, Cambridge CB2 1EZ, UK. Fax: +44 1223 336 408; e-mail: deposit@ccdc.cam.ac.uk or on the web: http://www.ccdc.cam.ac.uk.

Appendix A. Supplementary material

Supplementary data associated with this article can be found, in the online version, at http://dx.doi.org/10.1016/j.molstruc.2014.01.079.

References

[1] E. Hadjoudis, M. Vitterakis, I.M. Mavridis, Tetrahedron 43 (1987) 1345–1360.
[2] X.X. Xu, X.Z. You, Z.F. Sun, X. Wang, H.X. Liu, Acta Crystallogr. C 50 (1994) 1169–1171.
[3] L. Feringa, W.F. Jager, B. De Lange, Tetrahedron 49 (1993) 8267–8310.
[4] I. Willner, S. Rubin, Angew. Chem. Int. Ed. Engl. 35 (1996) 367.
[5] M. Jalali-Heravi, A.A. Khandar, I. Sheikshoaie, Spectrochim. Acta Part A Mol. Biomol. Spectrosc. 55 (1999) 2537–2544.
[6] O.M. Yaghi, G. Li, H. Li, Nature 378 (6558) (1995) 703–706.
[7] C.T. Chen, K.S. Suslick, Coord. Chem. Rev. 128 (1–2) (1993) 293–322.
[8] D. Mahadevan, S. Periandy, M. Karabacak, S. Ramalingam, N. Puviarasan, Spectrochim. Acta A 86 (2012) 139–151.
[9] A. Kovacs, V. Izvekov, G. Keresztury, G. Pongor, Chem. Phys. 238 (1998) 231–243.
[10] T. Tanaka, A. Nakajima, A. Watanabe, T. Ohno, Y. Ozaki, Vib. Spectrosc. 34 (2004) 157–167.
[11] Stoe & Cie, X-AREA (Version 1.18) Stoe & Cie, Darmstadt, Germany, 2002.
[12] Stoe & Cie (2002) X-RED32 (Version 1.04). Stoe & Cie, Darmstadt, Germany.
[13] G.M. Sheldrick, Acta Crystallogr. A 64 (2008) 112–122.
[14] L.J. Farrugia, J. Appl. Cryst. 30 (1997) 565–566.
[15] L.J. Farrugia, J. Appl. Cryst. 32 (1999) 837–838.
[16] A.L. Spek, J Appl. Cryst. 36 (2003) 7–13.
[17] M.J. Frisch, G.W. Trucks, H.B. Schlegel, G.E. Scuseria, M.A. Robb, J.R. Cheeseman, G. Scalmani, V. Barone, B. Mennucci, G.A. Petersson, H. Nakatsuji, M. Caricato, X. Li, H.P. Hratchian, A.F. Izmaylov, J. Bloino, G. Zheng, J.L. Sonnenberg, M. Hada, M. Ehara, K. Toyota, R. Fukuda, J. Hasegawa, M. Ishida, T. Nakajima, Y. Honda, O. Kitao, H. Nakai, T. Vreven, J.A. Montgomery Jr., J.E. Peralta, F. Ogliaro, M. Bearpark, J.J. Heyd, E. Brothers, K.N. Kudin, V.N. Staroverov, R.Kobayashi, J. Normand, K. Raghavachari, A. Rendell, J.C. Burant, S.S. Iyengar, J. Tomasi, M. Cossi, N. Rega, J.M. Millam, M. Klene, J.E. Knox, J.B. Cross, V. Bakken, C. Adamo, J. Jaramillo, R. Gomperts, R.E. Stratmann, O. Yazyev, A.J. Austin, R. Cammi, C. Pomelli, J.W. Ochterski, R.L. Martin, K. Morokuma, VG Zakrzewski, G.A. Voth, P. Salvador, J.J. Dannenberg, S. Dapprich, A.D. Daniels, O. Farkas, J.B. Foresman, J.V. Ortiz, J. Cioslowski, D.J. Fox, Gaussian 09, Revision A.1, Gaussian Inc., Wallingford CT, 2009.
[18] R. Dennington, T. Keith and J. Millam Semichem Inc., Shawnee Mission KS, GaussView, Version 5, 2009.
[19] C. Lee, W. Yang, R.G. Parr, Phys. Rev. B37 (1988) 785–789.
[20] A.D. Becke, J. Chem. Phys. 98 (1993) 5648–5652.
[21] P. Perdew, K. Burke, M. Ernzerhof, Phys. Rev. Lett. 77 (1996) 3865–3878.
[22] M.J. Frisch, J.A. Pople, J.S. Binkley, J. Chem. Phys. 80 (1984) 3265–3269.
[23] M.H. Jamróz, J.C.z. Dobrowolski, J. Mol. Struct. 565–566 (2001) 475–480.

[24] R. Ditchfield, J. Chem. Phys. 56 (1972) 5688–5691.
[25] I. Moustakali-Mavridis, E. Hadjoudis, A. Mavridis, Acta Crystallogr. Sect. B 34 (1978) 3709–3715.
[26] J.P. Merrick, D. Moran, L. Radom, J. Phys. Chem. A 111 (2007) 11683–11700.
[27] V. Balachandran, S. Lalitha, S. Rajeswari, Spectrochim. Acta Part A Mol. Biomol. Spectrosc. 91 (2012) 146–157.
[28] A. Teimouri, A.N. Chermahini, K. Taban, H.A. Dabbagh, Spectrochim. Acta A 72 (2009) 369–377.
[29] H.A. Dabbagh, A. Teimouri, A.N. Chermahini, M. Shahraki, Spectrochim. Acta A 69 (2008) 449–459.
[30] M. Govindarajan, K. Gansan, S. Periandy, S. Mohan, Spectrochim. Acta 76A (2010) 12–21.
[31] N.B. Colthup, L.H. Daly, S.E. Wiberly, Introduction to Infrared and Raman Spectroscopy, Academic Press, New York, 1990.
[32] T. Schlick, Molecular Modeling and Simulation: An Interdisciplinary Guide, second ed., Springer, New York, 2010. vol.21.
[33] D. Avcı, Y. Atalay, Struct. Chem. 20 (2009) 185–201.
[34] K. Pihlaja, E. Kleinpeter, Carbon-13 Chemical Shifts in Structural and Sterochemical Analysis, VCH Publishers, Deerfield Beach, 1994.
[35] H.O. Kalinowski, S. Berger, S. Braun, Carbon-13 NMR spectroscopy, John Wiley & Sons, Chichester, 1988.
[36] K. Fukui, Science 218 (1982) 747–754.
[37] M. Dinçer, D. Avcı, M. Şekerci, Y. Atalay, J. Mol. Mod. 14 (2008) 823–832.
[38] D. Avcı, Spectrochim. Acta A 82 (2011) 37–43.
[39] M. Yıldız, Z. Kılıc, T. Hokelek, J. Mol. Struct. 441 (1998) 1–10.
[40] P. Politzer, J.S. Murray, Theor. Chem. Acc. 108 (2002) 134–142.
[41] F. Weinhold, C. Landis, Valency and Bonding: A Natural Bond Orbital Donor–Acceptor Perspective, Cambridge University Press, Cambridge, 2005.
[42] L.T. Cheng, W. Tam, S.H. Stevenson, G.R. Meredith, G. Rikken, S.R. Marder, J. Phys. Chem. 95 (1991) 10631–10643.
[43] P. Kaatz, E.A. Donley, D.P. Shelton, J. Chem. Phys. 108 (1998) 849–856.
[44] R. Zhang, B. Dub, G. Sun, Y. Sun, Spectrochim. Acta A 75 (2010) 1115–1124.